Journal of Membrane Science 461 (2014) 59–68

Contents lists available at ScienceDirect

Journal of Membrane Science

journal homepage: www.elsevier.com/locate/memsci

Influence of polybenzimidazole main chain structure on H_2/CO_2 separation at elevated temperatures

Xin Li [a], Rajinder P. Singh [b], Kevin W. Dudeck [b], Kathryn A. Berchtold [b], Brian C. Benicewicz [a,*]

[a] Department of Chemistry and Biochemistry, University of South Carolina, Columbia, SC 29208, USA
[b] Carbon Capture and Separations for Energy Applications (CaSEA) Labs, Material Physics and Application Division, Los Alamos National Laboratory, Los Alamos, NM 87545, USA

ARTICLE INFO

Article history:
Received 13 October 2013
Received in revised form
27 February 2014
Accepted 5 March 2014
Available online 15 March 2014

Keywords:
Polybenzimidazole
Gas separation
Synthesis gas
Hydrogen separation membrane
Pre-combustion carbon capture

ABSTRACT

Four polybenzimidazole (PBI) derivatives were prepared to study the effects of main chain chemistry and structure on H_2/CO_2 perm-selectivity of cast films. These structural variations were designed to exhibit high localized mobility at elevated temperatures, contain rigid and bent configurations that frustrated close chain packing, or possess bulky side groups. The modified PBIs exhibited high molecular weights, slightly lower thermal stabilities, and higher organo-solubilities compared with commercial m-PBI. Dilute polymer solutions (< 3.0 wt%) were used to fabricate high quality thin films under carefully optimized film processing conditions. Gas permeation properties of these PBI films were evaluated at elevated temperatures (up to 250 °C) and pressures (up to 50 psia). It was found that the main chain structural variations effectively disrupted the PBI chain packing resulting in much improved film H_2 permeability (up to 997.2 barrer) compared with m-PBI (76.81 barrer) at 250 °C and 50 psia. However, lower H_2/CO_2 selectivities (5–7 (modified PBIs) versus 23 (m-PBI)) were also measured and reflected the general trade-off between gas permeability and selectivity. When tested at 250 °C, PBI-based materials exhibited gas separation performance higher than the Robeson upper bound prediction and are promising materials for high temperature H_2 separation from syngas.

© 2014 Elsevier B.V. All rights reserved.

1. Introduction

H_2 is a fast-growing market not only because of its significant applications in traditional areas such as ammonia production and oil refining but also its great potential as a clean energy carrier for renewable energy devices such as fuel cells and to address issues related to the world's oil consumption and environmental concerns [1–4]. As a result, great attention has been placed on improving H_2 production technologies with lower cost and higher efficiency. Although there are a variety of novel approaches for hydrogen production such as photoelectrochemical water splitting and biological H_2 production processes being explored, for the foreseeable future, hydrocarbon fuels such as natural gas and coal will remain the dominant methods for industrial H_2 production [5–8].

H_2/CO_2 separation is a critical step in hydrocarbon fuel processing for clean H_2 production while mitigating CO_2 emissions in electricity, power and fuels production process schemes. In a typical hydrocarbon processing scheme for H_2 production, post water-gas-shift reaction ($CO+H_2O \rightarrow CO_2+H_2$), synthesis (syn) gas is separated into H_2 and CO_2 rich streams. Industry standard H_2/CO_2 separation techniques are highly energy inefficient due to high parasitic energy losses associated with syngas heating and cooling, and sorbent regeneration [9,10]. Therefore, in recent years considerable research has been focused on investigating novel H_2/CO_2 separation technologies which could achieve improvements in both economics and performance [11–14].

Polymer membrane-based gas separation has emerged as a promising alternative to replace or use in combination with conventional gas separation techniques which could lead to processes that are more cost-effective, efficient, and less energy-intensive [15,16]. One widely recognized challenge that exists with polymer membrane based separation approaches is the trade-off relationship between gas permeability and selectivity. However, an increasing number of studies have shown that both gas permeability and selectivity characteristics can be improved through new polymer material design and/or polymer structure modification [17]. A successful gas separation membrane must also be applicable to industrially realistic gas processing conditions

* Corresponding author. Tel.: +1 803 777 0778; fax: +1 803 777 8100.
E-mail address: benice@sc.edu (B.C. Benicewicz).

http://dx.doi.org/10.1016/j.memsci.2014.03.008
0376-7388/© 2014 Elsevier B.V. All rights reserved.

including temperature, pressure, and tolerance to impurities while maintaining efficiency and providing economic benefit. H_2 selective membranes applicable for use under syngas processing conditions at high temperatures (>150 °C) are highly desirable since they would not require intermediate cooling procedures prior to treatment [18]. However, commercially available polymer membrane materials either do not meet these stability requirements or exhibit very poor gas separation performance at the desired elevated temperature condition.

Polybenzimidazoles (PBIs) are a class of heterocyclic polymers which possess extremely high thermal stability, excellent chemical and moisture resistance, and can be fabricated into fibers and films with outstanding mechanical stability [19,20]. For these reasons, PBIs have been widely studied in recent years as polymer electrolyte membrane (PEM) materials for high temperature fuel cell applications [21,22]. These properties also make PBI a promising candidate among the class of glassy thermoplastics in the application of H_2/CO_2 separation at elevated temperatures. Some preliminary work has been reported on evaluating the gas transport properties of commercially available poly(2,2′-(m-phenylene)-5,5′-bibenzimidazole) (m-PBI). For example, Pesiri et al. successfully prepared m-PBI meniscus membranes with an approximate thickness of 4 μm at the film centers and demonstrated H_2/CO_2 separations at elevated temperatures [23]. Berchtold et al. tested the long-term gas separation performance using m-PBI/zirconia/stainless steel composite membranes under pure and simulated dry syngas environments and reported good H_2/CO_2 selectivities and excellent thermo-chemical stability [24]. Kumbharkar et al. prepared m-PBI based hollow fiber membranes and measured the gas transport properties for H_2/CO_2 in the temperature range of 100–400 °C [25]. Although m-PBI exhibits industrially attractive H_2/CO_2 selectivity at elevated temperatures, its low H_2 permeability mandates ultrathin selective layer for commercially attractive H_2 fluxes. This low permeability is attributed to the small free volume of m-PBI resulting from efficient polymer chain packing due to pi-pi stacking and strong H-bonding interactions [26,27]. Therefore, strategies to improve the hydrogen permeability while simultaneously maintaining high H_2/CO_2 selectivity are needed to make this class of materials more industrially attractive.

Molecular structure modification is an effective way to manipulate aspects of polymer morphology such as chain packing efficiency and free volume architecture and to ultimately tune the gas diffusivity within the glassy polymers [28]. During the past few decades, tremendous work has been done on modifying the structures of known polymers such as polyimides to achieve a better balance between gas permeability and selectivity [29,30]. Although PBI represents a large family of heterocyclic polymers with the benzimidazole ring in its polymer repeat unit, very little work has been focused on investigating the structure-property relationships within this type of materials, especially with detailed studies of their corresponding gas separation characteristics at elevated temperatures [26,27].

In this work, PBI polymers with different backbone structures have been prepared using four different dicarboxylic acid monomers and evaluated as films for high-temperature H_2/CO_2 separations. PBI main chain molecular structure variation strategies to manipulate fractional free volume for controlling H_2 permselectivity were explored. These structural variations were designed to exhibit high localized mobility at elevated temperatures, contain rigid and bent configurations that frustrated close chain packing, or possess bulky side groups. A detailed study of their corresponding physicochemical properties was conducted and the results illustrate that PBI main chain structural modification is an effective method to increase the gas permeability at elevated temperatures. The gas transport properties of these new PBI derivatives were compared to the commercially available m-PBI material.

2. Experimental

2.1. Materials

2,2-Bis(4-carboxyphenyl)-hexafluoropropane (6F-diacid, 98.0%) was purchased from TCI America. 4,4′-((1,2,3,3,4,4-Hexafluorocyclobutane-1,2-diyl)bis(oxy))dibenzoic acid (PFCB-diacid, 99.0%) was obtained from Tetramer Technologies (distributed through Oakwood Chemical, Columbia, SC). 2,2′-Bis(trifluoromethyl)benzidine (98.5%) used in BTBP-diacid synthesis was purchased from Akron Polymer Systems. 1,1,3-Trimethyl-3-phenylindan-4′,5-dicarboxylic acid (phenylindane-diacid, 98%) was purchased from Amoco Chemicals. 3,3′,4,4′-Tetraaminobiphenyl (TAB, polymer grade, ~97.5%) was donated by BASF Fuel Cell, Inc. Polyphosphoric acid (PPA, 115%) was purchased from InnoPhos. The m-PBI used in this study as the benchmark PBI material was obtained from PBI Performance Products, Inc. and used as received. All other reagents (e.g. sodium cyanide, sodium nitrite, lithium chloride, etc.) and solvents (e.g. N,N-dimethylacetamide (DMAc), ammonium hydroxide, etc.) were purchased from Fisher Scientific. Unless otherwise specified, all chemicals were used without further purification.

2.2. PBI polymer synthesis

The detailed synthetic procedures of 2,2′-bis(trifluoromethyl)-4,4′-biphenyldicarboxylic acid (BTBP-diacid) and four different PBI variants (6F-PBI, PFCB-PBI, BTBP-PBI, and phenylindane-PBI) were reported previously [31–34]. Herein, 6F-PBI is used as an example to describe the general synthetic procedure of PBI polymers. To a 100 ml, three-necked, round-bottom flask, TAB (1.071 g, 5 mmol) and 6F-diacid (1.961 g, 5 mmol) were added under nitrogen protection in a glove box, followed by approximately 98.0 g PPA. The reactor was then equipped with an overhead mechanical stirrer and a nitrogen purge. The reaction mixture was stirred at 50 rpm under N_2 purge during the entire reaction procedure. The reaction temperature was controlled by a programmable temperature controller with ramp and soak capabilities. The typical final polymerization temperatures were 195–220 °C for 10–40 h. As the reaction proceeded, the solution developed a dark brown color and became viscous. At the end of the reaction, the polymer solution was poured into water to stop the reaction, pulverized in a blender, neutralized with ammonium hydroxide, filtered, washed with water, and dried in a vacuum oven at 110 °C to obtain the final 6F-PBI polymer powders.

2.3. PBI dense film preparation

The general free-standing polymer film casting procedure for the PBI derivatives is described as follows. To a 100 ml round-bottom flask, 1.00 g (applied to 6F-PBI, PFCB-PBI, and phenylindane-PBI) or 0.500 g (applied to BTBP-PBI) dry PBI powder and approximately 33 ml DMAc were added. The reaction mixture was heated to reflux at ca. 180 °C (oil bath temperature) for 3–4 h until most of the PBI powder was dissolved. The PBI solution was then cooled down to ambient temperature and centrifuged at 5500 rpm for 30 min to remove any undissolved or swollen polymer. The clean, brown color PBI solution was then transferred to a glove bag with nitrogen purge. The PBI solution was poured on a clean glass substrate (in the case of BTBP-PBI, the polymer solution is very dilute, so a glass substrate with glass slides taped on each side was used to restrict the movement of the solution) and heated to 40–50 °C on a hot-plate overnight to remove the solvent. Then, the glass plate was transferred to the vacuum oven and heated at 110 °C for 24–48 h to obtain the final dry, dense PBI films.

2.4. Characterization

^{1}H NMR and ^{19}F NMR spectra were recorded on a Varian Mercury 400 spectrometer. FT-IR spectra were recorded on a PerkinElmer Spectrum 100 FT-IR spectrometer with a three reflection diamond/ZnSe crystal. PBI inherent viscosities (IVs) were measured by a Cannon Ubbelohde viscometer with a 0.2 g/dL PBI solution in concentrated sulfuric acid (96%) at 30.0 °C. Thermogravimetric analysis (TGA) was conducted on polymer powders using a TG 209 F1 Iris from Netzsch Inc. The samples were heated at 200 ºC for 12 h to ensure residual solvent and adsorbed water removal prior to thermal analysis. After the drying step, samples were heated at a ramp rate of 2 °C/min in N_2 from 75 to 1000 °C. The densities of the PBIs were measured with a Kimble® Kimax® specific gravity bottle using cyclohexane as the solvent at 30.0 °C and a Micromeritics Accupyc 1330 gas displacement pycnometer using 99.999% purity helium at ambient conditions. The detailed gravity bottle density measurement protocols are presented in the supporting information. PBI powder and cast film samples were used for density measurement using the gravity bottle and gas pycnometer, respectively. The PBI film samples were annealed at 100 and 250 °C in a vacuum oven for 24 h prior to density measurement. The same samples were subjected to annealing at two temperatures with cool down to 30 °C under vacuum and density measurement in between the two annealing steps. PBI solubilities were measured at both ambient and reflux conditions. For ambient temperature solubility testing, the PBI powders were mixed with each solvent and shaken on a wrist action shaker for 24–48 h. For elevated temperature solubility testing, the PBI powders were mixed with each solvent and refluxed for 2–4 h.

2.5. Gas permeation testing

The PBI membranes were tested in a custom stainless steel housing using high temperature o-rings (Kalrez™) in a constant-volume variable-pressure test system. The module was configured for continuous feed gas flow using a dip tube and use of vacuum on the permeate side of the module housing for the permeance measurement. The pure gas permeation experiments were performed with H_2, CO_2, and N_2 at feed pressures and operating temperatures from 20 to 50 psi and 30 to 250 °C, respectively. A 1 °C/min temperature ramp rate was typically used in this work for both ramp-up and ramp-down cycles. The permeability data reported here was collected during temperature ramp-down cycle following a 10 h dwell at 250 °C. The upstream and downstream pressures were measured using high accuracy (± 0.25% FS) pressure transducers (MKS Instruments, Inc.). The permeance (GPU = 10^{-6} cm^3 cm^{-2} cmHg^{-1} s^{-1}) was calculated from the slope of the linear part of the permeate pressure rise versus time curve using Eq. (1):

$$\text{Permeance,}\quad P = 10^{6}\frac{dp}{dt}\left(\frac{V \times 22400}{RT\Delta pA}\right) \tag{1}$$

where dp/dt (Torr/s) is the pressure rise; R (62.363 Torr L K^{-1} mol^{-1}) is the universal gas constant, V (L) is the downstream volume; Δp (cmHg) is the pressure difference between membrane upstream and downstream side; T(K) is the permeate temperature; and A (cm^2) is the effective membrane surface area. The permeability was calculated using film thickness measured using scanning electron microscopy after testing. The ideal selectivity for a gas pair is calculated by taking the ratio of their gas permeances.

3. Results and discussion

3.1. Polymer synthesis and characterization

3.1.1. Polymer synthesis

As shown in Fig. 1, five different PBI variants were synthesized for the gas separation study. For comparison, m-PBI was obtained commercially (PBI Performance Products, Inc.) in both powder form (100 mesh PBI powders) and solution form (26.2 wt% PBI solution in N,N-dimethylacetamide (DMAc) containing 2 wt% lithium chloride as a phase stabilizer). Industrially, m-PBI is produced by a two-stage melt-solid polycondensation reaction (Fig. 1a) which is more convenient for large-scale production but usually produces lower molecular weight polymer due to the heterogeneous reaction conditions. The other four PBI variants were synthesized in this study by solution polymerization (Fig. 1b) in either PPA or Eaton's reagent. The solution polymerization in PPA is a convenient laboratory procedure for many PBIs since PPA serves as both solvent and condensation reagent and can produce high molecular weight polymer. This PPA-based procedure produced high molecular weight 6F-PBI and phenylindane-PBI. However, this procedure did not work for the synthesis of PFCB-PBI or BTBP-PBI as the PFCB-diacid monomer showed low PPA solubility

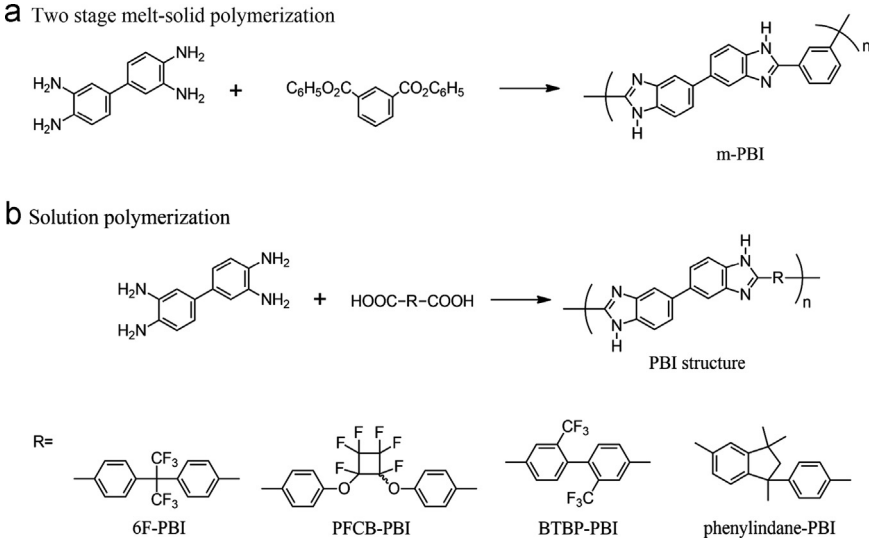

Fig. 1. Synthetic schemes of PBI derivatives (a. m-PBI; b. 6F-PBI, PFCB-PBI, BTBP-PBI, and phenylindane-PBI).

Table 1
Polymerization conditions of PBI derivatives.

Polymer	HOOC–R–COOH	Polymerization solvent	Monomer charge	Polymerization temperature (°C)	Polymerization time (h)	IV (dL g^{-1})
6F-PBI	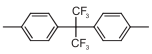	PPA	2.89 wt%	220	24	1.4
PFCB-PBI	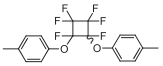	Eaton's Reagent[a]	1 mmol:5 ml[b]	140	24	0.73
BTBP-PBI	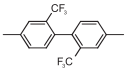	Eaton's Reagent[a]	1 mmol:5.5 ml[b]	140	42	1.6
phenylindane-PBI	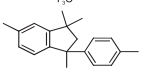	PPA	6.11 wt%	195	35	0.8

[a] Eaton's Reagent: a solvent mixture of methanesulfonic acid (MA) and phosphorous pentoxide (PP) (MA:PP = 10:1, w-w).
[b] *x* mmol:*y* ml: means *x* mmol each monomer dissolved in *y* ml Eaton's Reagent.

and BTBP-PBI appeared to cross-link in PPA at elevated temperatures. Thus, these two PBIs were prepared using Eaton's reagent as a convenient alternative to PPA. One important criterion for PBI synthesis is the polymer molecular weight (or IV) since high IV PBIs typically exhibit improved thermal stability and film forming properties in comparison to their lower IV analogs. The detailed discussion and optimization of PBI polymerization conditions was reported previously [31–34] and the general conditions used in this study are given in Table 1. 6F-PBI, PFCB-PBI, BTBP-PBI, and phenylindane-PBI were prepared with IVs of 1.40, 0.73, 1.60, and 0.81 dL/g, respectively, indicating relatively high polymer molecular weights. PBI structures were confirmed by FTIR, ^{1}H NMR and ^{19}F NMR and the spectra can be found in the Supplementary material.

3.1.2. Thermal properties

PBI thermal stability was studied using TGA under N_2. Polymer powders were pre-treated at 200 °C for 12 h in the TGA to remove residual solvents and absorbed water. As shown in Fig. 2, all PBIs exhibited excellent thermal stabilities and no obvious weight losses (> 1 wt%) were observed at temperatures up to 300 °C, a common feature of PBI polymers. Decomposition temperatures at different weight losses (1 wt%, 5 wt%, and 10 wt%) are given in Table 2. It was found that all four modified PBI derivatives exhibited lower thermal stabilities than m-PBI, which was likely caused by the introduction of less stable functional groups (e.g. polar groups, hydrocarbon rings, etc.) or the strong disruption of the chain pi–pi stacking and H-bonding interactions. However, all PBIs were stable enough for the desired gas permeation testing conditions (up to 250 °C).

3.1.3. Density

The density values obtained on PBI polymers synthesized in this work using gravity bottle and gas displacement pycnometry on powder and cast film samples after vacuum drying at 100–110 °C are in close agreement except for phenylindane-PBI, Table 2. In the case of phenylindane-PBI, a lower density value was observed for the cast film as compared to the powder sample. However, the density of phenylindane-PBI film increased after annealing at 250 °C. This density increase upon annealing at higher temperature might be indicative of residual solvent and water removal and/or structural rearrangement. It is anticipated that polymer processing history, especially in the case of PBI-based polymers due to their tight chain packing, can have significant effect on the polymer physical characteristics. The densities of all cast films were also measured after annealing at 250 °C in vacuum oven for 24 h. The density differences obtained after annealing

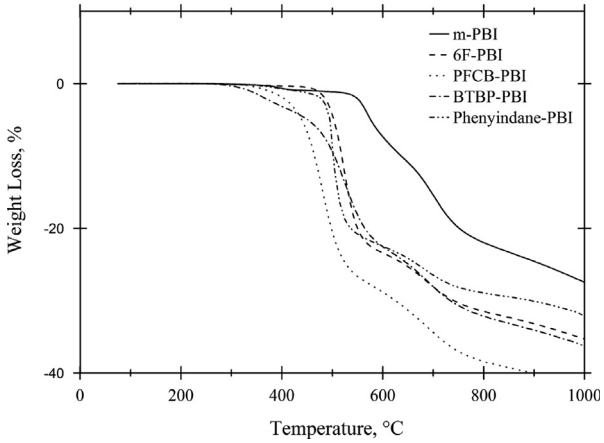

Fig. 2. TGA thermograms for PBI derivatives in N_2.

at 100 and 250 °C were small except for phenylindane-PBI as discussed above.

3.1.4. Solubility

PBI solubility characteristics were determined under two different dissolution conditions (a. 1.5 wt% polymer concentrations at ambient temperature; b. 3.0 wt% polymer concentration at reflux temperature) and the results are given in Table 3. At ambient conditions, all PBIs exhibited complete or partial dissolution in polar aprotic solvents such as DMAc and DMF. The modified PBI derivatives demonstrated improved solubility compared to m-PBI, which was attributed to the introduction of bulky, high mobility or twisted functional groups into the polymer backbones. At elevated temperatures, all PBIs showed improved solubility in DMAc and LiCl/DMAc at the higher solids concentration. However, for BTBP-PBI, the polymer solution in DMAc was found to exhibit poor long-term stability. BTBP-PBI precipitation was observed and the homogeneous solution became a swollen gel after sitting for 2–3 h at ambient conditions. Decreasing the polymer concentration or adding lithium chloride as a phase stabilizer was found to suppress the phase separation [33]. All PBIs were insoluble in common organic solvents such as acetone, THF, or MeOH.

3.2. PBI dense film preparation

Free-standing dense PBI films with thicknesses ranging from 5 μm to 20 μm were fabricated for pure gas permeation measurements. Several important factors potentially affecting the film quality

Table 2
Physical properties of PBI polymers.

Polymer	Density (g cm^{-3})			FFV[d]	Decomposition temperature (°C)[e]		
	Method a[a]	Method b[b]	Method c[c]		1.0 wt%	5.0 wt%	10.0 wt%
m-PBI	1.37	1.28	1.31	0.145	463	576	637
6F-PBI	1.41	1.44	1.44	0.145	474	507	523
PFCB-PBI	1.45	1.47	1.43	0.175	373	439	465
BTBP-PBI	1.47	1.52	1.52	0.098	355	488	500
Phenylindane-PBI	1.16	0.95	1.21	0.142	424	490	502

[a] Density data of PBI powders measured by specific gravity bottle after annealing the sample at 110 °C in vacuum oven overnight.
[b] Density data of PBI films measured by gas displacement pycnometry after annealing the samples in vacuum oven for 24 h at 100 °C.
[c] Density data of PBI films measured by gas displacement pycnometry after annealing the samples in vacuum oven for 24 h at 250 °C.
[d] Fractional free volume (FFV) calculated using polymer densities obtained from method c and Bondi's group contribution approach [35,36].
[e] Temperature where the noted weight loss percentage was observed.

Table 3
Solubility characteristics of PBI derivatives.

Polymer	Ambient Temperature							Reflux Temperature	
	DMAc	LiCl/DMAc	NMP	DMF	Acetone	THF	MeOH	DMAc	LiCl/DMAc
m-PBI (100 mesh)	+	+	+	+	−	−	−	++	++
6F-PBI	++	++	++	++	−	−	−	++	++
PFCB-PBI	++	++	++	++	−	−	−	++	++
BTBP-PBI	++	++	++	++	−	−	−	++*	++
Phenylindane-PBI	++	++	++	++	−	−	−	++	++

DMAc: N,N-dimethylacetamide; LiCl/DMAc: 4 wt% LiCl in DMAc; NMP: N-methyl-2-pyrrolidinone; DMF: dimethylformamide; THF: tetrahydrofuran; MeOH: methanol.
++: Mostly soluble; ++*: mostly soluble, but polymer precipitated after cooling; +: partially soluble or swelling; −: insoluble.

and gas permeation characteristics were studied. These factors included humidity, LiCl stabilizer, and solvent evaporation rate.

3.2.1. Humidity

It was noted that the PBI solution systems (PBI/DMAc or PBI/LiCl/DMAc) were very hygroscopic and thus, for the films cast and dried in the open air, water from the surrounding environment was absorbed by the polymer solutions and caused phase separation in the PBI films. As a result, the PBI polymer precipitated prematurely and formed a porous film with large pores and voids. These features both reduced the film mechanical properties and gas separation performance. Fig. 3 (left) shows an example of a 6F-PBI film cast in the open air where the film opacity was a direct result of the strong phase separation. To eliminate the influence of humidity, the PBI films were cast and dried under dry nitrogen in a glove bag, and then transferred to a vacuum oven. The final film, as shown in Fig. 3 (right), was much stronger and transparent, indicating that a high-quality PBI dense film was formed.

3.2.2. LiCl addition

The addition of LiCl to the PBI/DMAc solution has been commonly used in PBI processing to improve both the polymer solubility and solution stability. It was postulated that Li^+ cation could react with DMAc to form a $[DMAc+Li]^+$ macrocation, thus allowing the Cl^- anion more freedom to disrupt the intra- and inter-molecular hydrogen bonding and suppress PBI aggregation in solution [37–39]. Therefore, LiCl was added to the PBI/DMAc solution for initial film casting studies. It was found that even a small amount of LiCl added to the 6F-PBI solution (6F-PBI: LiCl=1:0.3, w-w) caused the cast film (LiCl was washed out by boiled water) (Fig. 3 (middle)) to become translucent and much weaker than the film cast from pure DMAc (Fig. 3 (right)). It is proposed that LiCl aggregation may occur during the solvent evaporation and subsequently affect the polymer morphology,

Fig. 3. 6F-PBI free-standing films prepared by various methods (left: prepared with 3 wt% 6F-PBI/DMAc solution in open air; middle: prepared with 3 wt% 6F-PBI/LiCl/DMAc (PBI:LiCl=1:0.3, w-w) under dry nitrogen protection; right: prepared with 3 wt% 6F-PBI/DMAc solution under dry nitrogen protection).

although a detailed mechanism study is still under investigation. In this work, pure DMAc was chosen as the solvent to eliminate the influence of LiCl and obtain accurate correlations between PBI structure and gas permeation properties.

3.2.3. Rate of evaporation

The film drying procedure in this study was divided into two stages: (1) the initial solvent evaporation in a glove bag under dry nitrogen and (2) final heating in a vacuum oven. It was found the initial solvent evaporation speed in a nitrogen environment greatly affected the film quality. For PBIs such as PFCB-PBI, a high initial heating temperature (75–110 °C, hot-plate temperature) resulted in defects such as patterns or uneven thickness in the films. Therefore, lower heating temperatures (40–50 °C, hot-plate temperature) were applied and homogeneous films could be routinely prepared. Fig. 4 shows the fabrication strategy that

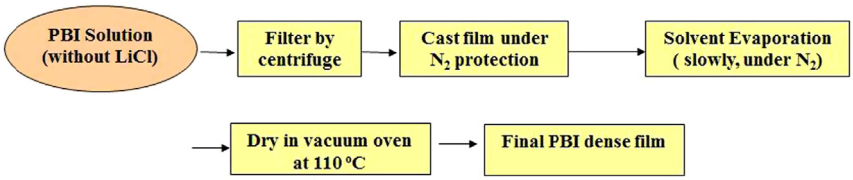

Fig. 4. Optimized PBI dense film preparation conditions.

Table 4
Perm-selectivity for the PBI membrane derivatives tested at 250 °C and 50 psia.

Polymers	Pure gas permeance (GPU)			Pure gas permeability (barrer)			Pure gas selectivity		E_p (kJ mol^{-1})[a]		
	H_2	CO_2	N_2	H_2	CO_2	N_2	H_2/CO_2	H_2/N_2	H_2	CO_2	N_2
6F-PBI	162.1	31.34	8.661	997.2	192.7	53.26	5.174	18.72	8.36	0.391	11.02
BTBP-PBI	89.07	12.53	3.802	710.4	99.91	30.33	7.111	23.43	10.94	4.275	13.62
Phenylindane-PBI	24.55	3.765	0.9329	480.6	73.69	18.26	6.522	26.32	10.39	3.107	14.01
PFCB-PBI	22.55	3.415	0.9617	323.1	48.92	13.79	6.604	23.45	13.1	6.715	17.64
m-PBI	3.564	0.1548	0.03625	76.81	3.335	0.7812	23.03	98.32	19.35	17.05	27.48

[a] E_p is the activation energy of the permeabilities obtained from the slope of permeability versus inverse temperature.

facilitated the fabrication of PBI films for all the polymers tested which resulted in consistent quality for gas permeation studies.

3.3. Gas transport properties

3.3.1. Membrane fundamentals

In an ideal gas separation model, when the upstream pressure (p_1) is significantly larger than downstream pressure (p_2), the permeability (P) of penetrant gas through a dense polymer membrane can be expressed as the product of the diffusion coefficient (D) and solubility coefficient (S) as shown in Eq. (2):

$$P = DS \tag{2}$$

By calculating the permeability ratio of two different gases, for instance P_{H_2}/P_{CO_2} in this work, the ideal gas selectivity (α_{H_2/CO_2}) is obtained, providing an assessment of the polymer film's ability to separate these gases from a mixed gas system. Also according to Eq. (2), when factoring the permeability into diffusivity and solubility, the ideal H_2/CO_2 selectivity can be obtained from the product of the mobility selectivity (D_{H_2}/D_{CO_2}) and sorption selectivity (S_{H_2}/S_{CO_2}) as shown in Eq. (3):

$$\alpha_{H_2/CO_2} = \frac{P_{H_2}}{P_{CO_2}} = \left[\frac{D_{H_2}}{D_{CO_2}}\right]\left[\frac{S_{H_2}}{S_{CO_2}}\right] \tag{3}$$

In general, the mobility selectivity of polymer films to separate gas mixtures is based on their ability to act as "molecular sieves". Therefore, the polymer film preferentially transports the smaller sized H_2 molecules (kinetic diameter=2.89 Å) rather than the larger CO_2 molecules (kinetic diameter=3.30 Å). Comparatively, the sorption selectivity of polymer films is mainly determined by the relative gas condensabilities (or gas critical temperature/boiling point), so CO_2 (boiling point=195 K) usually exhibits higher solubility than H_2 (boiling point=20 K) in polymeric membranes. Generally in glassy polymers, large segmental chain movements are relatively limited so gas diffusion plays the dominant role in deciding the overall gas transport properties. Therefore, in this specific application, increasing penetrant mobility and mobility selectivity in the polymers are the most important criteria to design commercially attractive H_2-selective polymeric membranes.

3.3.2. Gas permselectivity at elevated temperatures

The pure gas permselectivities of the PBI derivatives tested at 250 °C and 50 psia are reported in Table 4. For m-PBI, the H_2 permeance is 3.6 GPU (3.6×10^{-6} cm^3 cm^{-2} s^{-1} cm Hg^{-1}) and the H_2/CO_2 and H_2/N_2 ideal selectivities are 23.0 and 98.3, respectively. The PBI film thicknesses were measured using SEM after gas permeation testing. The film thickness of m-PBI was approximately 21.6 μm and thus, the corresponding H_2 permeability is 76.8 barrer (76.8×10^{-10} cm^3 cm cm^{-2} s^{-1} cm Hg^{-1}). Previously Berchtold et al. reported H_2 permeability of 58 barrer and H_2/CO_2 selectivity of 43 for m-PBI [24]. They evaluated a PBI/ceramic composite membrane for one year at 250 °C. The effects of long term membrane exposure to elevated temperature are likely the major contributing factor in the observed differences in H_2 permselectivity characteristics measured in this work as compared to that reported by Berchtold et al. The lower H_2 permeability and higher H_2/CO_2 selectivity reported there are consistent with polymer structure tightening due to long term exposure to elevated temperatures.

As shown in Table 4, all the modified PBIs exhibited significantly higher gas permeabilities than m-PBI, indicating the chain functionalization effectively changed the polymer chain packing (e.g. free volume architecture) and ultimately improved the gas transport properties. The H_2 permeability of 6F-PBI was 997.2 barrer (997.2×10^{-10} cm^3 cm cm^{-2} s^{-1} cm Hg^{-1}) at 250 °C, which was approximately 13× higher than m-PBI and was also the highest among all the synthesized PBI derivatives. PBI gas permeabilities correlated well with gas molecule size (kinetic diameter: H_2 (2.89 Å) < CO_2 (3.30 Å) < N_2 (3.64 Å)), indicating that a diffusion-based selectivity (or size sieving effect) plays the dominant role in the gas transport properties at elevated temperatures. The polymer densities were measured by pycnometry at ambient temperature after annealing the film samples at 250 °C and used for polymer fractional free volume (FFV) calculations (Table 2). No direct correlation was found between FFV data and polymer gas transport characteristics. Numerous factors including polymer FFV, molecular weight, gas–polymer interactions, and polymer glass transition temperature in relation to operating temperature (i.e., polymer molecular mobility at use conditions) influence the gas transport characteristics of polymer materials. The interplay between these influencing factors and convolution of their ultimate property influences makes one-to-one chemistry–property or structure–property relationship identification a daunting task. Further targeted chemistry–structure–property relationship exploration, building on

the work presented here, is required to gain additional insight and specificity regarding the complex interplay of influencing factors in these PBI-based materials.

This work explored several strategies for PBI main chain modifications with the goal of increasing polymer gas permeability. In general, these strategies or factors are correlated so it is difficult to isolate one effect from the others. For instance, incorporating bulky and rigid functional moieties could help to "stiffen" the chain and decrease the chain packing efficiency (i.e. increase free volume), which would generally increase gas diffusivity. However, these rigid functionalities could also increase the energy barrier for, and thus restrict, chain torsional mobility which would lead to decrease in gas diffusivity. One example of this complex interplay of influencing factors is observed in the comparison of 6F-PBI and PFCB-PBI. Both of these materials possess bulky and relatively flexible chain connectors compared with m-PBI. As a result, both 6F-PBI and PFCB-PBI have, as anticipated, significantly higher H_2 permeability than m-PBI. Based on the calculated FFVs for these same polymers alone, it is anticipated that PFCB-PBI would exhibit a higher H_2 permeability. However, in practice the H_2 permeability of PFCB-PBI is lower than that of 6F-PBI. This permeability differential is attributed to the increased rigidity of the PFCB functionality over that of the 6F functionality. A second illustrative example is found in the comparison of BTBP-PBI with phenylindane-PBI. The BTBP-PBI has a rigid-rod but also twisted backbone conformation (caused by the steric repulsion of bistrifluoromethyl groups), which suppresses the chain packing efficiency. Phenylindane-PBI possesses a bulky, rigid bent moiety in the polymer backbone which could also decrease chain packing density. The calculated FFVs for BTBP-PBI and phenylindane-PBI are both lower than that calculated for m-PBI indicating tighter chain packing. However, the higher H_2 permeability of BTBP-PBI and phenylindane-PBI indicates contrary. Therefore, further quantitative and direct FFV analysis of PBI-based polymers using analytical techniques such as positron annihilation lifetime spectroscopy (PALS) is required to further correlate gas permselectivity characteristics with polymer microstructure.

The increase in H_2 permeability resulted in a significant decrease of ideal gas selectivities for all the modified PBIs. The H_2/CO_2 selectivity decreased from 23 (m-PBI) to approximately 5–7 (all other PBIs), indicating a much more open chain packing structure for the modified PBIs.

3.3.3. *Effect of temperature on gas permselectivity*

The effect of operating temperature on gas permselectivities is very important since it can be used to attain an optimum set of permeability and selectivity characteristics and to select the proper materials for a specific application (e.g. H_2/CO_2 separation at elevated temperatures). m-PBI is considered a poor material for ambient temperature H_2 separation due to its low permeability [23]. This is attributed to the extremely tight and close chain packing characteristics of m-PBI caused by strong pi-pi interactions and interchain hydrogen bonding. However, the rigid structure and excellent thermal resilience of m-PBI make it promising candidate for H_2/CO_2 separation at extreme conditions [23]. For polymer materials, the temperature dependence of the gas diffusion coefficient and solution coefficient can be expressed as follows (Eqs. (4) and (5)):

$$D = D_0 e^{-E_d/RT} \tag{4}$$

$$S = S_0 e^{-\Delta H_s/RT} \tag{5}$$

where E_d is the activation energy of diffusion; ΔH_s is the partial molar enthalpy of sorption; D_0 and S_0 are constants; R is the universal gas constant; and T is the operating temperature. In general, the diffusion coefficient increases with temperature whereas the solubility coefficient decreases with temperature, i.e. E_d is positive and ΔH_s is negative. For glassy PBI polymers, diffusion coefficients are strongly dependent on temperature with minimal solubility contributions to permeability. Thus, their

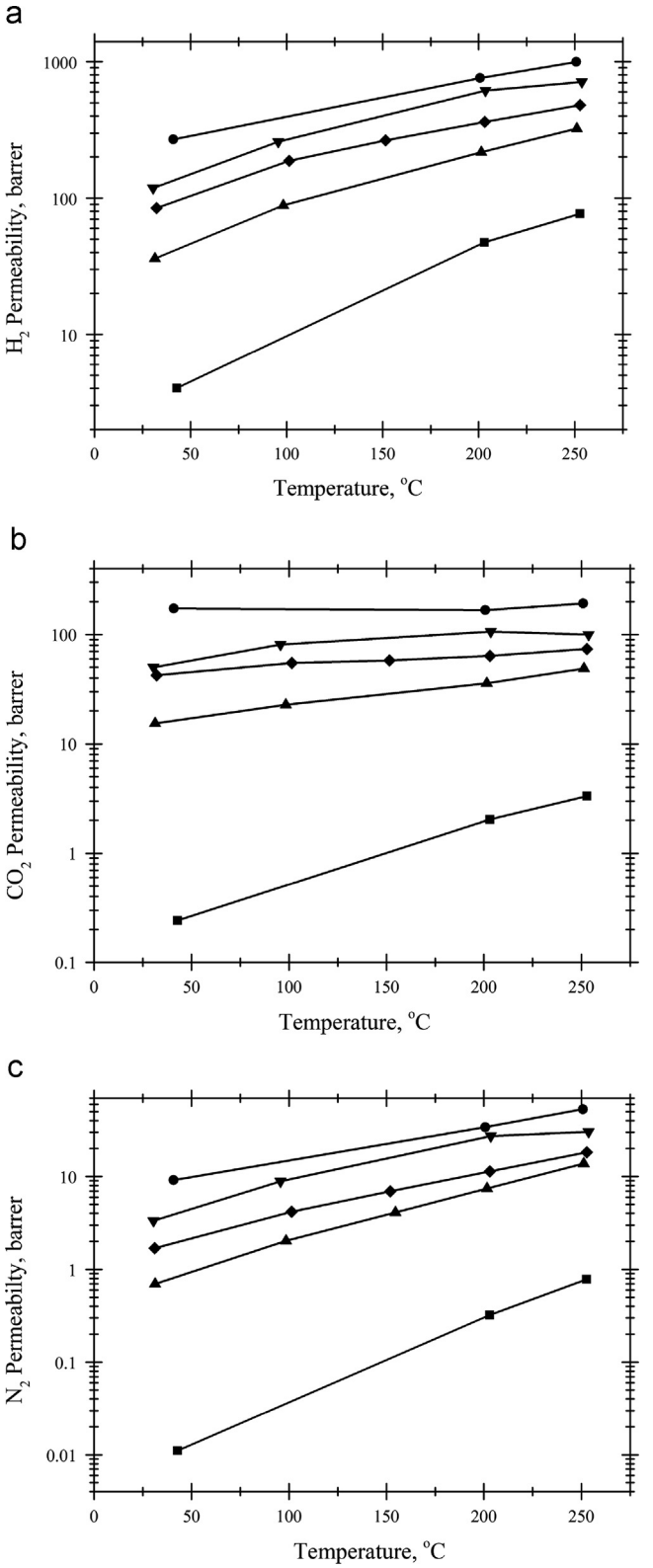

Fig. 5. Effect of operating temperature on pure gas permeabilities ((a) H_2; (b) CO_2; (c) N_2) of PBI derivative membranes (circles: 6F-PBI; downtriangles: BTBP-PBI; diamonds: phenylindane-PBI; uptriangles: PFCB-PBI; squares: m-PBI). The lines are drawn to guide the eye.

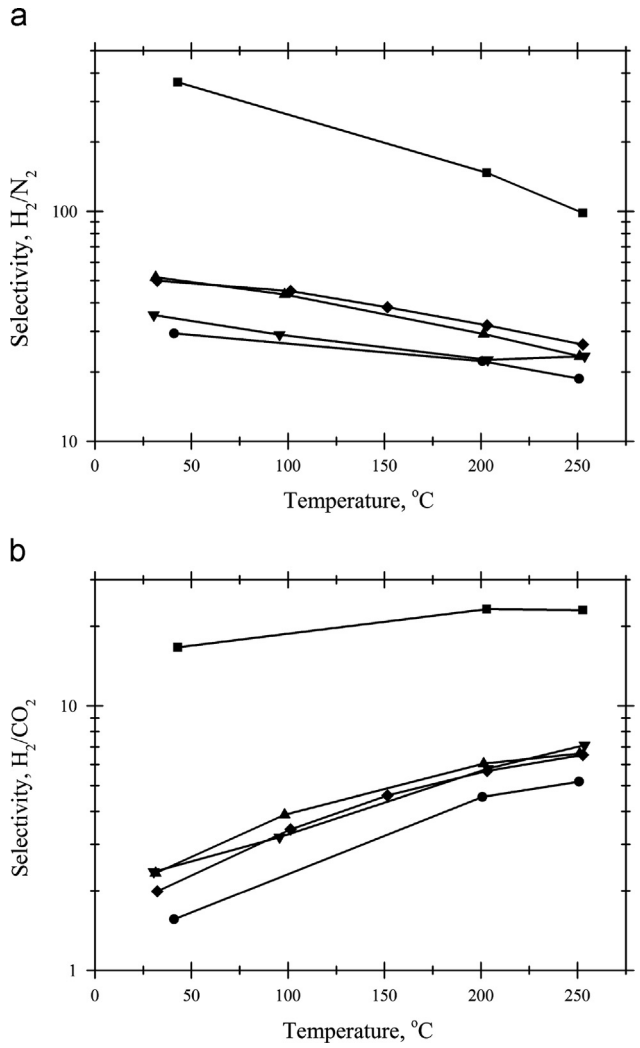

Fig. 6. Effect of operating temperature on H_2/N_2 (a) and H_2/CO_2 (b) ideal selectivities of the PBI derivative membranes (circles: 6F-PBI; down-triangles: BTBP-PBI; crystals: phenylindane-PBI; up-triangles: PFCB-PBI; squares: m-PBI). The lines are drawn to guide the eye.

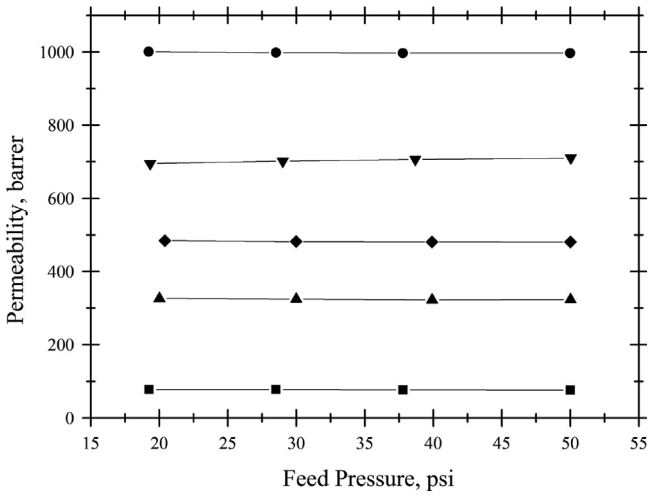

Fig. 7. Effect of trans-membrane pressure on the H_2 permeability of the PBI derivative membranes (circles: 6F-PBI; down-triangles: BTBP-PBI; crystals: phenylindane-PBI; up-triangles: PFCB-PBI; squares: m-PBI). The lines are drawn to guide the eye.

permeability behavior is typically consistent with activated diffusion, i.e., as operating temperature increases all gas diffusivity coefficients increase resulting in increased gas permeabilities. Fig. 5 shows the temperature dependence of the gas permeabilities (H_2, CO_2, and N_2) for all the PBI derivatives. It was found that the gas permeabilities of all PBIs increased with temperature, indicating a diffusion-dominated gas transport mechanism in the temperature range tested. The activation energy of permeability (E_p) was calculated from this data and the results are shown in Table 4. The order of E_p is $N_2 > H_2 > CO_2$ indicating greatest influence of temperature on N_2 permeability.

Fig. 6 shows the temperature dependence of the ideal selectivities for H_2/N_2 (a) and H_2/CO_2 (b) for the evaluated polymers. The selectivity of glassy polymers often decreases with temperature as less permeable gas component often possesses higher activation energies, i.e., these less permeable gases realize relatively larger increases in permeability with increasing temperature. The temperature dependence of the ideal H_2/N_2 selectivity for these PBI membranes follows this general trend. Furthermore, the polymer chain motion (rotational and vibrational) is significantly influenced at elevated temperatures. Since polymer free volume is a function of polymer chain packing and inter-segmental motion, the increased N_2 permeability is also influenced by the effect of elevated temperature on these aforementioned polymer macromolecular characteristics. In contrast, the H_2/CO_2 ideal selectivities increase with temperature indicating that the increase in H_2 permeability as a function of temperature is greater than that of CO_2. The effect of temperature on permeability is quantitatively shown in the values of E_p (Table 4), which are significantly larger for H_2 than for CO_2. The large increase in H_2 permeability compared to that of CO_2 with temperature is attributed to its smaller size consistent with the size sieving characteristics of PBI. In addition, the solubility driven permeability component, the minor component in these PBI materials, is expected to be higher for CO_2 as compared to H_2 due to higher CO_2 solubility in the polymer. However, this solubility component will decrease with increasing temperature thereby further contributing to an increase in H_2/CO_2 selectivity.

An exception to the general increase in permeability as a function of temperature is observed for 6F-PBI membrane. In contrast to the other PBI-derivatives studied here, as the operating temperature is increased from near-ambient to 250 °C, the CO_2 permeability remained nearly constant for 6F-PBI membranes. This 6F-PBI membrane behavior can be attributed to strong CO_2–polymer interactions in this highly fluorinated material combined with its activated diffusion character. In general, CO_2 has significantly higher solubility in polymers as compared to H_2 and N_2 due to dipole–dipole interaction between CO_2 and the polymer [40]. This CO_2-polymer interaction is expected to be significant for 6F-PBI due to presence of highly electronegative 6F group. However, the gas solubility decreases as temperature increases (Eq. (5)). Therefore, the solubility contribution to permeability decreases while the diffusivity contribution increases with operating temperature. This interplay between diffusivity and solubility results in a near constant 6F-PBI CO_2 permeability over the evaluated temperature range.

3.3.4. *Effect of pressure on gas permselectivity*

The relationship between gas permeability and transmembrane pressure was also investigated. Fig. 7 shows the H_2 permeability at 250 °C for the PBIs at different trans-membrane pressures from 20 to 50 psi. A fairly constant H_2 permeability was observed for all of the polymers, indicating the absence of viscous flow and correspondingly, defects in the tested dense membranes.

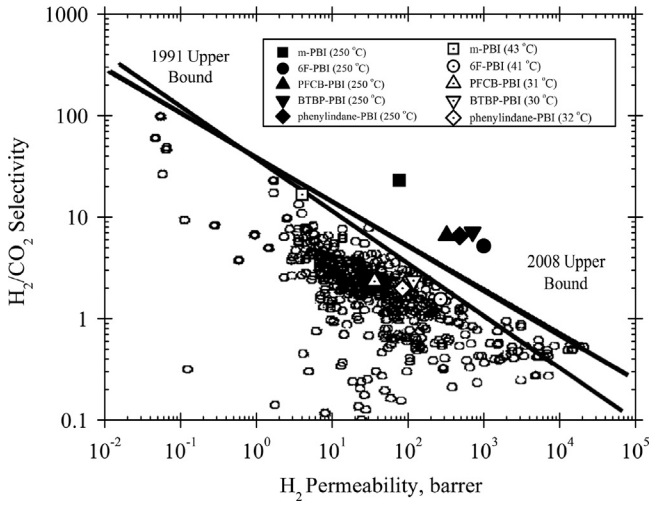

Fig. 8. Robeson plot comparing the PBI derivative membranes with other polymeric membranes tested for the H_2/CO_2 separation. The lines represents the 1991 and 2008 Robeson upper bounds and the open circles represent literature data for polymeric gas separation membranes [17].

3.3.5. *Comparison to other polymeric membranes*

As discussed previously, the gas separation performance of polymeric membrane materials is generally subjected to a trade-off relationship between gas permeability and gas selectivity. Tremendous work has been done on exploring the gas separation performance of various kinds of polymeric materials in the past few decades and these experimental results were collected and organized by Robeson to draw a series of upper-bound curves based on different gas pairs [17,41]. Fig. 8 shows Robeson's upper-bound curve for the H_2/CO_2 gas pair published in 2008. Polymeric materials with gas separation capabilities surpassing the upper-bound and located in the upper right hand quadrant of Fig. 8 are considered as attractive candidates for H_2/CO_2 separation. However, the literature data shown in Fig. 8 by Robeson were acquired at relatively low temperature (35 °C). While the use of near-ambient temperature conditions is a standard test protocol, it does not provide sufficient information to assess the technical viability of a membrane for H_2/CO_2 separation at typically encountered syngas processing conditions. Very few data or reports could be found in the literature for H_2/CO_2 separation at elevated temperatures (>150 °C) largely due to the low thermal degradation temperatures of most polymer-based materials. The gas separation performance of the PBIs evaluated in this work at both ambient temperature and 250 °C was incorporated into the H_2/CO_2 Robeson plot (Fig. 8). The permselectivities of all PBIs at 250 °C exceeded the Robeson upper bound indicating the potential utility of these PBI-based materials for H_2 separation from syngas at elevated temperatures. However, more effort is required to further optimize this class of materials for industrially attractive H_2/CO_2 separations.

4. Conclusion

A series of high molecular weight PBI derivatives with modified bulky/flexible/frustrated backbone structures were successfully synthesized by solution polymerization in PPA or Eaton's Reagent and compared to commercially available m-PBI for H_2/CO_2 gas separation. The modified PBIs exhibited slightly decreased thermal stabilities and better organo-solubilities compared to m-PBI, which was attributed to the ability of the various functional groups to "open up" or disrupt the polymer chain packing. The PBI derivatives were fabricated into free-standing films by solution casting. Film casting protocols were optimized to optimize film quality, including mechanical properties and defect levels. H_2/CO_2 separation testing was performed on the cast membranes at temperatures ranging from ca. 30 °C to 250 °C and varied pressure. It was found that the PBI films exhibited improved gas separation properties (H_2 permeability and H_2/CO_2 selectivity) with an increase in operating temperature. Also, the introduction of bulky/flexible/frustrated functionalities into the PBI backbone effectively disrupted the polymer close chain packing and provided materials with much higher H_2 permeability (up to 997.2 barrer) compared to m-PBI (76.81 barrer) at 250 °C. However, decreases in H_2/CO_2 selectivities from 23.03 (m-PBI) to 5–7 (other PBIs) were also observed at 250 °C in these materials. No direct correlations were found between the calculated FFV data and the gas separation characteristics within the PBI derivatives. All PBIs exhibited elevated temperature (250 °C) gas separation performance exceeding the Robeson upper-bound, indicating their promise for application as membranes for H_2 purification from syngas.

Acknowledgments

This project supports the U.S. DOE Energy Efficiency and Renewable Energy – Advanced Manufacturing Office – Industrial Technologies Program. The authors gratefully acknowledge the U.S. DOE/EERE for financial support of the project under Contract CPS #18990. Los Alamos National Laboratory is operated by Los Alamos National Security, LLC for DOE/NNSA under Contract DE-AC52-06NA25396. The authors also acknowledge PBI Performance Products Inc. for their programmatic contributions.

Appendix A. Supplementary material

Supplementary data associated with this article can be found in the online version at http://dx.doi.org/10.1016/j.memsci.2014.03.008.

References

[1] G. Marbán, T. Valdés-Solís, Towards the hydrogen economy? Int. J. Hydrog. Energy 32 (2007) 1625–1637.
[2] J.A. Turner, Sustainable hydrogen production, Science 305 (2004) 972–974.
[3] A. Midilli, M. Ay, I. Dincer, M.A. Rosen, On hydrogen and hydrogen energy strategies I: current status and needs, Renew. Sust. Energy Rev. 9 (2005) 255–271.
[4] P.P. Edwards, V.L. Kuznetsov, W.I.F. David, Hydrogen energy, Philos. Trans. R. Soc. A—Math. Phys. Eng. Sci. 365 (2007) 1043–1056.
[5] J. Turner, G. Sverdrup, M.K. Mann, P.C. Maness, B. Kroposki, M. Ghirardi, R. J. Evans, D. Blake, Renewable hydrogen production, Int. J. Energy Res. 32 (2008) 379–407.
[6] S.K. Ngoh, D. Njomo, An overview of hydrogen gas production from solar energy, Renew. Sust. Energy Rev. 16 (2012) 6782–6792.
[7] R.M. Navarro, M.A. Pena, J.L.G. Fierro, Hydrogen production reactions from carbon feedstocks: fossils fuels and biomass, Chem. Rev. 107 (2007) 3952–3991.
[8] J.D. Holladay, J. Hu, D.L. King, Y. Wang, An overview of hydrogen production technologies, Catal. Today 139 (2009) 244–260.
[9] E.S. Rubin, H. Mantripragada, A. Marks, P. Versteeg, J. Kitchin, The outlook for improved carbon capture technology, Prog. Energy Combust. Sci. 38 (2012) 630–671.
[10] A.A. Olajire, CO_2 capture and separation technologies for end-of-pipe applications – A review, Energy 35 (2010) 2610–2628.
[11] D. Grainger, M.-B. Hägg, Techno-economic evaluation of a PVAm CO_2-selective membrane in an IGCC power plant with CO_2 capture, Fuel 87 (2008) 14–24.
[12] G. Krishnan, D. Steel, K.C. O'Brien, R. Callahan, K.A. Berchtold, J.D. Figueraa, Simulation of a process to capture CO_2 from IGCC syngas using a high temperature PBI membrane, Energy Proc. 1 (2009) 4079–4088.
[13] H. Li, Z. Song, X. Zhang, Y. Huang, S. Li, Y. Mao, H.J. Ploehn, Y. Bao, M. Yu, Ultrathin, molecular-sieving graphene oxide membranes for selective hydrogen separation, Science 342 (2013) 95–98.
[14] H. Lin, E. Van Wagner, B.D. Freeman, L.G. Toy, R.P. Gupta, Plasticization-enhanced hydrogen purification using polymeric membrane, Science 311 (2006) 639–642.

[15] S.A. Stern, Polymers for gas separations – the next decade, J. Membr. Sci. 94 (1994) 1–65.
[16] K. Ghosal, B.D. Freeman, Gas separation using polymer membranes: an overview, Polym. Adv. Technol. 5 (1994) 673–697.
[17] L.M. Robeson, The upper bound revisited, J. Membr. Sci. 320 (2008) 390–400.
[18] T.C. Merkel, M. Zhou, R.W. Baker, Carbon dioxide capture with membranes at an IGCC power plant, J. Membr. Sci. 389 (2012) 441–450.
[19] H. Vogel, C.S. Marvel, Polybenzimidazoles, new thermally stable polymers, J. Polym. Sci. 50 (1961) 511–539.
[20] A.S. Buckley, D.E. Stuetz, G.A. Serad, Encycl. Polym. Sci. Eng. 11 (1987) 572–601.
[21] J.T. Wang, R.F. Savinell, J. Wainright, M. Litt, H. Yu, A H-2/O-2 fuel cell using acid doped polybenzimidazole as polymer electrolyte, Electrochim. Acta 41 (1996) 193–197.
[22] L. Xiao, H. Zhang, E. Scanlon, L.S. Ramanathan, E.W. Choe, D. Rogers, T. Apple, B.C. Benicewicz, High-temperature polybenzimidazole fuel cell membranes via a sol–gel process, Chem. Mater. 17 (2005) 5328–5333.
[23] D.R. Pesiri, B. Jorgensen, R.C. Dye, Thermal optimization of polybenzimidazole meniscus membranes for the separation of hydrogen, methane, and carbon dioxide, J. Membr. Sci. 218 (2003) 11–18.
[24] K.A. Berchtold, R.P. Singh, J.S. Young, K.W. Dudeck, Polybenzimidazole composite membranes for high temperature synthesis gas separations, J. Membr. Sci. 415 (2012) 265–270.
[25] S.C. Kumbharkar, Y. Liu, K. Li, High performance polybenzimidazole based asymmetric hollow fibre membranes for H_2/CO_2 separation, J. Membr. Sci. 375 (2011) 231–240.
[26] S.C. Kumbharkar, P.B. Karadkar, U.K. Kharul, Enhancement of gas permeation properties of polybenzimidazoles by systematic structure architecture, J. Membr. Sci. 286 (2006) 161–169.
[27] S.C. Kumbharkar, U.K. Kharul, Investigation of gas permeation properties of systematically modified polybenzimidazoles by N-substitution, J. Membr. Sci. 357 (2010) 134–142.
[28] Y. Yampolskii, I. Pinnau, B.D. Freeman (Eds.), Material Science of Membranes for Gas and Vapor Separation, John Wiley & Sons, Chichester, England, 2006.
[29] J.D. Wind, D.R. Paul, W.J. Koros, Natural gas permeation in polyimide membranes, J. Membr. Sci. 228 (2004) 227–236.
[30] Y. Liu, R. Wang, T.S. Chung, Chemical cross-linking modification of polyimide membranes for gas separation, J. Membr. Sci. 189 (2001) 231–239.
[31] G. Qian, B.C. Benicewicz, Synthesis and characterization of high molecular weight hexafluoroisopropylidene-containing polybenzimidazole for high-temperature polymer electrolyte membrane fuel cells, J. Polym. Sci. Part A: Polym. Chem. 47 (2009) 4064–4073.
[32] G. Qian, D.W. Smith Jr, B.C. Benicewicz, Synthesis and characterization of high molecular weight perfluorocyclobutyl-containing polybenzimidazoles (PFCB-PBI) for high temperature polymer electrolyte membrane fuel cells, Polymer 50 (2009) 3911–3916.
[33] X. Li, G. Qian, X. Chen, B.C. Benicewicz, Synthesis and characterization of a new fluorine-containing polybenzimidazole (PBI) for proton-conducting membranes in fuel cells, Fuel Cells 13 (2013) 832–842.
[34] X. Li, X. Chen, B.C. Benicewicz, Synthesis and properties of phenylindane-containing polybenzimidazole (PBI) for high-temperature polymer electrolyte membrane fuel cells (PEMFCs), J. Power Sources 243 (2013) 796–804.
[35] D.W. Van Krevelen, K. Te Nijenhuis, Properties of Polymers: Their Correlation with Chemical Structure; Their Numerical Estimation and Prediction From Additive Group Contributions, 4th edn., Elsevier, Amsterdam, 2009.
[36] A. Bondi, van der Waals Volumes and Radii, J. Phys. Chem. 68 (1964) 441–451.
[37] A.M. Striegel, Theory and applications of DMAC/LiCl in the analysis of polysaccharides, Carbohydr. Polym. 34 (1997) 267–274.
[38] A.M. Striegel, Advances in the understanding of the dissolution mechanism of cellulose in DMAc/LiCl, J. Chil. Chem. Soc. 48 (2003) 73–77.
[39] C.B. Shogbon, J.L. Brousseau, H. Zhang, B.C. Benicewicz, Y.A. Akpalu, Determination of the molecular parameters and studies of the chain conformation of polybenzimidazole in DMAc/LiCl, Macromolecules 39 (2006) 9409–9418.
[40] D.M. D'Alessandro, B Smit, J.R. Long, Carbon dixoide capture: prospects for new materials, Angew. Chem. Int. Ed. 49 (2010) 6058–6082.
[41] L.M. Robeson, Correlation of separation factor versus permeability for polymeric membranes, J. Membr. Sci. 62 (1991) 165–185.